In Algorithms for Synthetic Aperture Radar Imagery VI, SPIE 3721, Orlando, FL, Apr. 5-9, 1999.

Feature Extraction using Attributed Scattering Center Models on SAR Imagery *

Michael A. Koets and Randolph L. Moses

Department of Electrical Engineering, The Ohio State University

ABSTRACT

We present algorithms for feature extraction from complex SAR imagery. The features parameterize an attributed scattering center model that describes both frequency and aspect dependence of scattering centers on the target. The scattering attributes extend the widely-used point scattering model, and characterize physical properties of the scattering object. We present two feature extraction algorithms, an approximate maximum likelihood method that relies on minimization of a nonlinear cost function, and a computationally faster method that avoids the nonlinear minimization step. We present results of applying both algorithms on synthetic model data, on XPatch scattering predictions of the SLICY test target, and on measured X-band SAR imagery.

Keywords: synthetic aperture radar, feature extraction, scattering centers

1. INTRODUCTION

At high frequencies, the radar backscatter from an object is well-approximated as the sum of responses from individual scattering centers on the object. As a result, scattering center descriptions have been proposed as features for model-based automatic target recognition (ATR) in high-frequency SAR target classification systems. In this paper we adopt an *attributed scattering center* model as a representation of object backscatter in high frequency SAR imagery. The attributed scattering center model has recently been proposed;[1–3] it includes both frequency and aspect dependence of scattering by retaining dominant terms in electromagnetic scattering solutions of canonical objects.

We focus on feature extraction of attributed scattering model parameters from measured SAR imagery. We present algorithms that directly process SAR images to generates a list of physical characteristics of the scattering centers that make up the object. The parameter estimates are computed locally from data in high energy regions of the SAR image.

We present two algorithms for feature extraction. The first is an approximate maximum likelihood (ML) algorithm whose statistical accuracy is close to the Cramér-Rao bound. This algorithm uses nonlinear minimization techniques to refine initial parameter estimates. A second algorithm is computationally more efficient, and is a slight variant of the initial parameter estimation step of the ML algorithm. These two algorithms offer a choice between estimation accuracy and fast computation. Both algorithms incorporate automatic selection of model order and of scattering center type.

The algorithms presented here extend earlier developments with a number of improvements. Frequency-domain algorithms for parameter estimation[1] are effective at estimating parameters for a small numbers of scattering centers; however, these methods become computationally intensive for practical targets, because the number of scattering centers is large and the estimation does not decouple in the frequency domain, so all parameters must be estimated simultaneously. Image-domain methods[2] have been developed by transforming the attributed scattering center model into the SAR image domain. Image-domain processing offers the advantage that scattering centers decouple, so the estimation problem can be split into a number of smaller problems to lower computational cost. In order to convert the model into the image domain, however, a number of restrictive assumptions are made (such as small percent bandwidth of the radar). Our methods operate in the image domain, but perform data reconstruction from model parameters in the frequency domain; this reduces computation and avoids the restrictive assumptions needed convert the model to the image domain, but retains the local processing benefit of image-domain feature extraction. We also develop automated order and structure estimation methods that were not available in previous algorithms.

*This research was supported in part by DARPA and the Air Force Research Laboratory under Grant F33615-979191020. The views and conclusions contained in this document are those of the authors and should not be interpreted as representing the official policies, either expressed or implied, of the Defense Advanced Research Projects Agency or the United States Government.

Similar algorithms that operate in the image domain have been developed for a point scattering model.[4] The point scattering model is simpler than the one we employ, and lacks the rich description of scattering center geometry available in the model we use; it also requires less sophisticated order selection procedures.

We have applied our algorithms to several SAR image data sets. We demonstrate the capability of our algorithms to accurately describe the physical structure of a measured object by applying them to a simple geometric test target. We have also applied our feature extraction algorithms to SAR images of military vehicles that are distributed by the Moving and Stationary Target Acquisition and Recognition (MSTAR) program.[5]

2. ATTRIBUTED SCATTERING CENTER MODEL

We adopt a recently developed physically-based model for backscattered responses from objects measured at high frequencies.[2] The model approximates the scattering response by a sum of responses from individual scattering centers; each scattering center response is modeled using the dominant terms of monostatic scattering solutions from both Physical Optics and the Geometric Theory of Diffraction. The model incorporates both frequency and aspect dependence of scattering centers, and characterizes each scattering center by a set of parameters describing its location, amplitude, shape, and orientation. The model generalizes the widely-used point scattering model[4,6] which assumes scattering centers are isolated points whose responses are all identical, and are independent of frequency and angle. The proposed attributed scattering center model thus provides a concise, physically relevant description of the object and is thus good candidates for use in target recognition, radar data compression, and scattering phenomenology studies.

We assume that a complex-valued spotlight-mode SAR image is available as a measurement. Synthetic aperture radar illuminates a region measures the energy scattered back to the radar by objects in the region. The measurements consist of amplitude and phase of the returned signal at a number of frequencies uniformly spaced across a frequency band at uniformly spaced angles around the region.

The frequency-domain attributed scattering model is given by[2]

$$m(f,\phi;\theta) = \sum_{i=1}^{n} m_i(f,\phi;\theta_i) \tag{1}$$

where $\theta^T = [\theta_1^T, \ldots, \theta_n^T]$ and

$$m_i(f,\phi;\theta_i) = A_i \cdot \left(j\frac{f}{f_c}\right)^{\alpha_i} \exp\left(\frac{-j4\pi f}{c}(x_i\cos\phi + y_i\sin\phi)\right) \operatorname{sinc}\left(\frac{2\pi f}{c}L_i\sin(\phi-\overline{\phi_i})\right) \exp(-2\pi f\gamma_i\sin\phi) \tag{2}$$

Here, f is frequency, f_c is the radar center frequency, ϕ is aspect angle, and $c = 3\times10^8$ m/sec is the propagation velocity. Each $m_i(f,\phi;\theta_i)$ represents a scattering center. The parameters x_i and y_i are the downrange and crossrange locations, A_i is the scattering center amplitude, and $\alpha_i \in [-1, -0.5, 0, 0.5, 1]$ describes the frequency dependence.

The remaining three parameters (γ_i, L_i, and $\overline{\phi}_i$) define the angle dependence of the scattering. There are two types of scattering centers: localized and distributed. Localized scattering centers have localized returns in the SAR image, and include trihedrals, points, top hats, and spheres. Distributed scattering centers have responses that often span several image pixels, and include dihedrals, flat plate and cylinder broadside returns, and broadside edge diffraction. For localized scattering centers, $L_i = \bar{\phi}_i = 0$ and γ_i represents the (small) angle dependence of the response. For distributed scattering centers, $\gamma_i = 0$ and L_i models the length of the scattering center and $\bar{\phi}_i$ its orientation angle.

The parameters α and L in the model distinguish among several scattering geometries. Table 1 shows how the α and L parameters differentiate between several canonical scattering shapes.

3. FEATURE EXTRACTION ALGORITHMS

In this section we present the algorithms for estimating the parameters of our model in equations (1)–(2) for the scattering centers of a synthetic aperture radar image. We describe two algorithms, an approximate maximum likelihood (ML) method that employs nonlinear minimization to refine an initial estimate, and a second, computationally faster algorithm with lower accuracy. The algorithm sequentially estimates scattering centers from regions of local

Scattering Geometry	α	L
Dihedral	1	$L > 0$
Trihedral	1	$L = 0$
Cylinder	1/2	$L > 0$
Sphere	0	$L = 0$
Edge Broadside	0	$L > 0$
Edge Diffraction	$-\frac{1}{2}$	$L > 0$
Corner Diffraction	-1	$L = 0$

Table 1. Physical Interpretation of α and L Parameters

maxima in the image, starting with the highest amplitude one. For each region, we fit a small number of scattering centers to that region by first obtaining initial estimates, followed by nonlinear minimization on the parameter set to minimize a weighted quadratic fit error in the peak region of the image. The fast algorithm skips the iterative nonlinear refinement step. We subtract the reconstructed model from the original data. This models the region of interest and also removes sidelobes from the remainder of the image. If sidelobe leakage into other regions is not a problem, the regions can be processed in parallel rather than recursively. We model each local maximum, starting with the highest one, as a small number of scattering centers.

3.1. Segmentation and Order Selection

We employ a segmentation process based on a watershed algorithm to isolate regions of high energy in the image.[7] This algorithm is applied magnitude of the complex data. The algorithm operates by treating the magnitude image as a three-dimensional landscape under water; as the water is drained, local maxima surface and assigned a new segment number. The segments are "grown" as the water is drained until they meet other segments. Each segment corresponds to a region of local maximum, and we apply local feature extraction to each segment.

When forming regions, we initially combine any regions whose local minima are within η dB of the local maxima surrounding it. This avoids segmenting distributed scattering returns into multiple smaller regions. We keep track of local maxima in these combined regions, and if the region is classified as containing localized scattering centers, then multiple localized scatterers are modeled in that region, as discussed below.

In the fast algorithm we segment the region once and extract features from each segment. In the ML algorithm we start with the highest peak, and recursively estimate parameters and subtract the reconstructed model from the original image, in an approach based on the CLEAN method.[8] This allows us to remove sidelobes of strong scattering terms, whose energy is not localized to a small region.

After we isolate a segment of the SAR image, we determine to which class of scattering centers the segment of data belongs. We classify the segment as a distributed scattering center, a single localized scattering center, or multiple localized scattering centers by classifying the region using its moments of inertia about the vertical and horizontal axes. Let $D(i,j)$ be the magnitude image pixel for $i = 1, \ldots, N_v$ and $j = 1, \ldots, N_h$, and let $\tilde{D}(i,j)$ be $D(i,j)$ masked by the selected region; thus, pixels of $\tilde{D}(i,j)$ that do not correspond to pixels in the selected segment have values of zero. The center of mass of the segment is then computed in the vertical (C_v) and horizontal (C_h) directions by

$$C_v = \frac{\sum_{i=1}^{N_v}\sum_{j=1}^{N_h} i \cdot \tilde{D}(i,j)}{\sum_{i=1}^{N_v}\sum_{j=1}^{N_h} \tilde{D}(i,j)} \qquad C_h = \frac{\sum_{i=1}^{N_v}\sum_{j=1}^{N_h} j \cdot \tilde{D}(i,j)}{\sum_{i=1}^{N_v}\sum_{j=1}^{N_h} \tilde{D}(i,j)} \tag{3}$$

Similarly, the horizontal and vertical moments of inertia are computed by

$$I_v = \sum_{i=1}^{N_v}\sum_{j=1}^{N_h}(j - C_h)^2 \cdot \tilde{D}(i,j) \qquad I_h = \sum_{i=1}^{N_v}\sum_{j=1}^{N_h}(i - C_v)^2 \cdot \tilde{D}(i,j) \tag{4}$$

The ratio of I_v to I_h is used to discriminate between distributed scattering centers and localized scattering centers. Distributed scattering centers appear as relatively narrow, long features oriented in a roughly horizontal direction in the image, and have a higher value for I_v/I_h than do localized scattering centers. Single or multiple localized

scattering centers are usually clustered into a more circular region and will have I_v/I_h ratios that are near one for most SAR imaging geometries.

If a region is classified as a localized scattering region, local maxima within the region are used to determine if one or more than one scattering center is present. The method is simple and works well at high SNR; at lower SNR a more rigorous statistically-based model order estimation method (such as an MDL-based technique) could be used to improve performance.

3.2. Initial Parameter Estimates

We generate initial estimates of the parameters of the scattering centers in a selected segment. For each localized scattering center in the segment, we must estimate the parameter set $\{x, y, \alpha, \gamma, A\}$, and we need to estimate the set $\{x, y, \alpha, \overline{\phi}, L, A\}$ for a distributed scattering center. We compute initial estimates for these values from the measured data or assign initial values based on knowledge of the range of values that are reasonable to represent the scattering mechanisms. The amplitude term, A, is determined by a linear least squares fit once the other parameters have been estimated. These initial parameter estimates are the final result for the fast variant of the algorithm; for the ML algorithm, iterative minimization of a nonlinear cost criterion is applied to these initial estimates.

Estimating x and y

We initialize the x and y parameters for a localized scattering center as the center of mass of the region. We already compute the center of mass using equation (3) to classify the scattering, so there is no computational overhead. If the region contains p local maxima and is not classified as a distributed scattering center, we initialize the locations of the p localized scatterers at the maxima in the segment.

Estimating L

Distributed scattering mechanisms are described by the parameter L. We compute an initial estimate of L as follows. If $\bar{\phi} = \gamma \approx 0$, $f \approx f_x$, $f_x = f\cos\phi$, then from equation (2) we have

$$s(f_x, f_y) \approx A\left(j\frac{f_x}{f_c}\right)^{\alpha} \operatorname{sinc}\left(\frac{2\pi L}{c} y f_y\right) \exp\left(\frac{-j4\pi}{c} x f_x\right) \exp\left(\frac{-j4\pi}{c} f_y\right) \tag{5}$$

Because the DFT is separable, the 1-D Fourier transform of the crossrange image line passing through the scattering center is approximately equal to (with f_y sampled at values $\Delta \cdot v$ for integer v):

$$s(v) = K \exp\left(\frac{-j4\pi\Delta}{c} v\right) \operatorname{sinc}\left(\frac{2\pi L\Delta y}{c} v\right) \tag{6}$$

If we consider only the magnitude of this function and normalize it to have a peak value of 1, we have

$$g(v) = \left|\operatorname{sinc}\left(\frac{2\pi L\Delta}{c} v\right)\right| = \operatorname{sinc}\left(\frac{2\pi L\Delta}{c} v\right) \text{ for } \left|\frac{2\pi\Delta}{c} v\right| \leq \pi \tag{7}$$

We extract a one dimensional slice of the image in the cross range direction through the center of mass of the scattering center from the image. We set to zero all pixels in this slice that are not in the region containing the distributed scattering center. We compute one dimensional discrete Fourier transform of the data, remove the zero padding, and divide the result by the window used in image formation. We then compute the magnitude and normalize it to obtain a data set that is approximated by the model of equation (7).

We use a Taylor expansion around $v = 0$ to approximate the main lobe of the sinc with a quadratic function

$$\operatorname{sinc}\left(\frac{2\pi L\Delta}{c} v\right) \approx 1 - \frac{(2\pi L\Delta)^2}{6c^2} v^2 \tag{8}$$

With this approximation in mind we attempt to fit a function of the form $f(v) = 1 + av^2$ to the normalized points in the measured data set that correspond to the peak of the sinc function. We use all data points with values above 0.7 in the normalized measured data set for this process. If fewer than three points have values above 0.7, the three

data points with the largest magnitudes are selected. The value $v = 0$ corresponds to the peak pixel. We use find the value of a which minimizes the cost

$$E = \sum_{i \in P} d_i (d_i - (1 + a v_i^2))^2 \tag{9}$$

Here P corresponds to the set of pixels we selected and d_i is the value of the normalized measured data at the selected point. This cost function is a measure of the error between the data and the quadratic function in which more weight is given to points near the peak. We can solve for this value of $\hat{a}$ directly.

$$\hat{a} = \frac{\sum_{i \in P} d_i^2 v_i^2 - \sum_{i \in P} d_i v_i^2}{\sum_{i \in P} d_i v_i^4} \tag{10}$$

and compute the estimate for L as

$$\hat{L} = \frac{c\sqrt{-6\hat{a}}}{2\pi\Delta} \tag{11}$$

It is also possible to generate an estimate for the length of the scattering center by measuring the apparent length of the feature in the image domain. This method is reasonably accurate if the scattering center spans multiple pixels, but is not so accurate if the the distributed scattering center is only 2–3 pixels in extent. Thus, the image-domain algorithm works well for long scatterers or for high resolution imagery.

Estimating γ and $\overline{\phi}$

We initialize $\gamma = 0$. We also initialize $\overline{\phi} = 0$ in most cases. One can instead estimate $\overline{\phi}$ by either finding the angle corresponding to the maximum eigenvalue of the contour ellipses found from the best Gaussian fit to the region.[9] One can also estimate $\overline{\phi}$ from the location of the peak in $s(v)$ in equation (6) after removing the assumption that $\overline{\phi} \approx 0$. If iterative parameter refinement is used, we have found that the simpler $\overline{\phi} = 0$ initialization gives similar final estimates. One of the above alternatives may be used if the iterative refinement step is skipped.

Estimating α

We estimate α after the other parameters above have been estimated by testing each of the five possible values $\alpha \in [-1, -1/2, 0, 1/2, 1]$ and finding the one that gives the best model fit. If the region contains multiple scattering centers, this exhaustive trial may be computationally intensive; if p scattering centers are present, one must test 5^p cases. For small percent bandwidth data, α has high uncertainty in most cases,[2] and for the ML algorithm we have found that the much simpler initialization $\alpha = 0$ provides a good starting point for the iterative minimization in most cases.

Estimating A

Because the amplitude A, is linear in the measurement vector, we estimate it by linear least squares. After all the other model parameters have been selected we generate a SAR image from the model using those parameters and an amplitude of 1. The data in the specified region of the measured data and model image are selected and formed into vectors. We assume the simulated image and the measured data are related by

$$A \cdot \tilde{M} + \tilde{N} = \tilde{D} \tag{12}$$

Here $\tilde{M}$ is the vector of simulated data over the region, $\tilde{D}$ is the measured data over the region, $\tilde{N}$ is a noise vector, and A is a complex valued scalar. We can then employ a linear least squares technique to estimate the value of A as

$$\hat{A} = (\tilde{M}^H \tilde{M})^{-1} \tilde{M}^H \tilde{D} \tag{13}$$

We have implemented a second method of estimating A that produces a real-valued result. This estimate is computed by choosing A to be the scalar that, when multiplied by the magnitude of the peak in the region of the simulated image, equals the magnitude of the peak in the region of the measured image. This method is a more accurate means of estimating the amplitude when the fast variation of the algorithm is employed, because errors in the location parameter estimates can be large enough to make $\tilde{M}$ and $\tilde{D}$ in equation (12) dissimilar, resulting in $\hat{A} \approx 0$ from (13).

4. PARAMETER OPTIMIZATION

We apply nonlinear optimization techniques to refine the initial parameter estimates to obtain approximate maximum likelihood (ML) estimates under the assumption of additive Gaussian noise. We formulate a stochastic model for the data by assuming that the measurement, in the (f_x, f_y) plane, is the sum of evaluations of the model using several parameter sets and additive white Gaussian noise. Thus we have

$$D = \sum_{k=1}^{n} M_{\theta_k} + N = M_\Theta + N \tag{14}$$

where D is the measured data in the (f_x, f_y) plane, n is the number of scattering centers, M_{θ_k} is data produced by evaluating the model using the parameter set θ_k, M_Θ is the sum of the model evaluations using the parameter sets that describe each of the scattering centers, and N is a matrix of zero mean white Gaussian noise with covariance Σ. This accounts for sensor noise, clutter, model mismatch and interpolation artifacts. Since the image formation process is linear, the image domain measurement is sum of responses from individual scattering centers, and the noise is zero mean Gaussian, but with a different covariance matrix. The probability density function for the image vector of image pixels is thus given by

$$f_\Theta(\tilde{D}) = \frac{1}{\pi^K |\tilde{\Sigma}|} \exp\left[-(\tilde{D} - \tilde{M}_\Theta)^H \tilde{\Sigma}^{-1} (\tilde{D} - \tilde{M}_\Theta)\right] \tag{15}$$

Here $\tilde{D}$ is the $K \times 1$ image domain measurement vector, $\tilde{M}_\Theta$ is the image formed from the model data, and $\tilde{\Sigma}$ is the covariance matrix for the measurement vector in the image domain. The maximum likelihood estimates of the model parameters are defined as

$$\hat{\Theta}_{ML} = \arg\max_\Theta f_\Theta(\tilde{D}) = \arg\min_\Theta (\tilde{D} - \tilde{M}_\Theta)^H \tilde{\Sigma}^{-1} (\tilde{D} - \tilde{M}_\Theta) \tag{16}$$

We treat α as a continuous-valued parameter in the minimization, and quantize α to half-integer values at the end.

Maximum likelihood estimates of the parameters require minimizing the right hand side of equation (16) for all scattering centers simultaneously and using the entire image, $\tilde{D}$. We instead implement an approximation to the ML estimates by decomposing the image into several regions, each of which corresponds to a small number of scattering centers, and estimating the parameters of those scattering mechanisms individually. This approximation is good when the energy of the scattering centers is primarily contained within the isolated regions of the image. This is the case in the data we consider. In our implementation the $\tilde{M}_\Theta$ vector corresponds to a region of the image and the parameters in the vector Θ describe only one or a small number of scattering centers; we apply equation (16) recursively for each region, then subtract the modeled scattering centers from the image and estimate parameters from the next region using the residual image; we continue recursively until all scattering centers are estimated. For each minimization we use the BFGS Quasi-Newton method with gradient estimation.

5. EXPERIMENTAL RESULTS

This section describes experiments using a variety of simulated and measured synthetic aperture radar images. Three types of data have been used. First, synthetic scattering generated directly from the parametric model are used to validate the estimation algorithms when both the data and the noise fit the assumed model. Second, XPatch scattering predictions of the SLICY test object are used to test the algorithms under well-controlled conditions, and also permit us to study algorithm performance on higher resolution data than is currently available from field measurements. Finally, algorithms are tested with measured spotlight SAR X-band image chips of vehicles.

5.1. Parameter Estimation Results for Synthetic Model data

First, we tested the algorithms on synthetically-generated data of an isolated scattering center at 6 in resolution. We simulated an ideal trihedral and an ideal dihedral. We added Gaussian white noise to the frequency-domain scattering values, and tested the estimation accuracy of the feature extraction algorithms for various SNR values; here, SNR is defined as

$$SNR = 20 \log_{10}\left(\frac{P_I}{\sigma_I}\right) \tag{17}$$

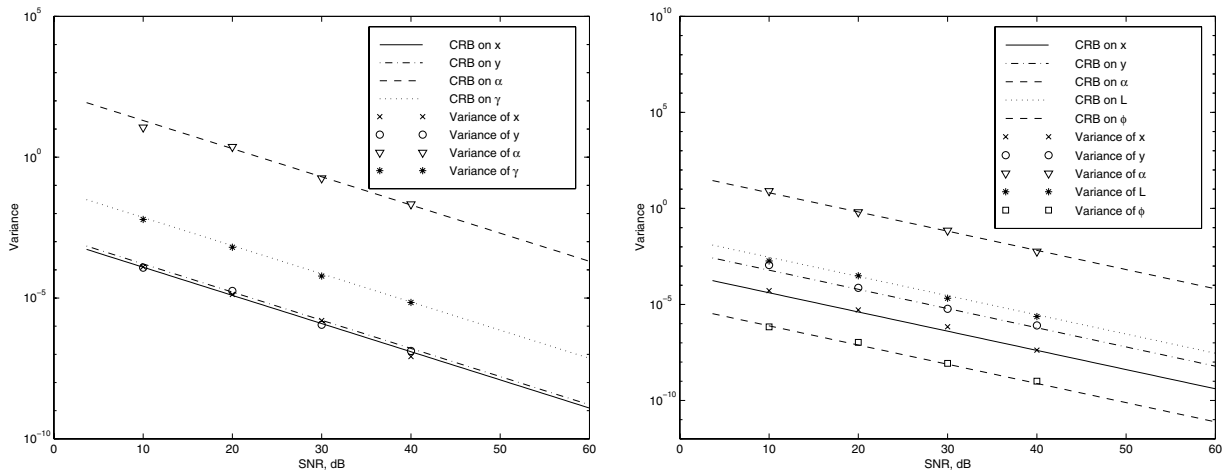

(a) (b)

Figure 1. Observed Variances of ML parameter estimation algorithm, for synthetic trihedral (a) and dihedral (b) at 6" resolution. Variances of x and y and L are in in^2 and variance of $\overline{\phi}$ is in rad^2 .

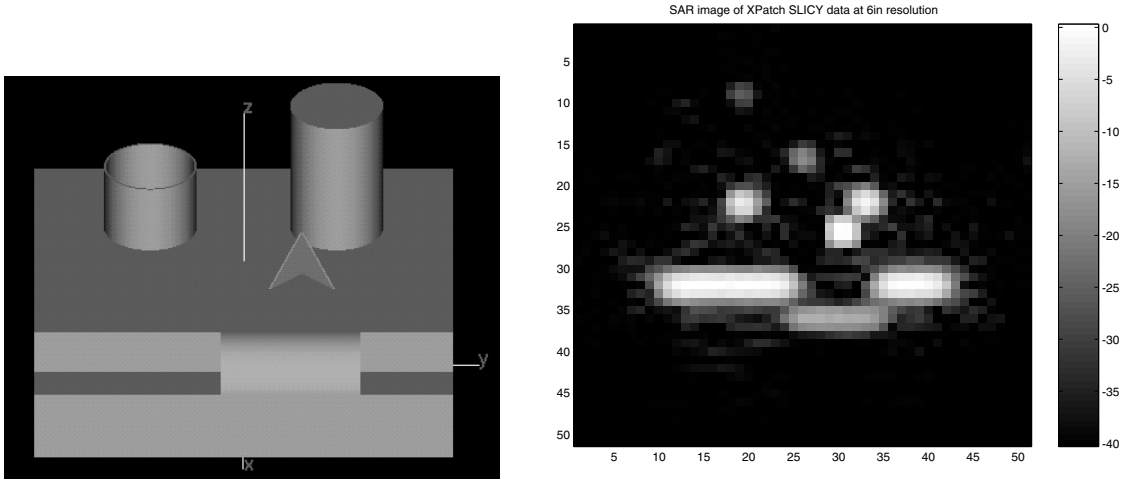

(a) (b)

Figure 2. CAD model of the SLICY target, and an example SAR image at 6 in resolution.

where P_I is the peak magnitude of the noiseless image of the scattering center and σ_I is the standard deviation of the noise in the image domain. We also compared the variances to the Cramér-Rao bound.[2,9] Figure 1 compares the estimated variances of from the ML estimator to the Cramér-Rao bounds. We see that the estimated parameters lie nearly on the Cramér-Rao bounds for all SNR values tested.

5.2. XPatch SLICY Results

We conducted experiments to evaluate the statistical properties of our algorithms using scattering predictions of the SLICY target using XpatchF. The SLICY target and an example SAR image are shown in Figure 2

Figure 3 shows parameter estimation results for the SLICY data at 6 in resolution and various levels of noise. The Cramér-Rao bound lines shown were computed using the parameters estimated from the noiseless data as the true parameter values. In most cases the ML algorithm generates estimates with variances near the bound. The most apparent exception is the variance of the estimates of the x parameter for the distributed scattering center. The

suboptimal variance in the estimates of this parameter is caused by limited precision of the numerical optimization routines that estimate the parameter values. While the estimates of the down range position have a variance above the bound, the variance is still very low; a 95% confidence interval on the down range position of ± 1 mm. The fast algorithm does not generally produce estimates with variances near the bound. However, the observed variances for this algorithm are low for many cases and would be adequate to accurately describe the scattering centers in practice. The fast algorithm produces estimates of α with variances below the bound for low SNR values because it only assigns values to this parameter drawn from a small set of half integer values, whereas the CRB is derived assuming a continuous α parameter.

In some cases the algorithms failed to correctly identify or classify the region. Both algorithms failed to correctly classify the localized scattering center in 14 of the 50 trials at 10 dB SNR, and 1 trial at 20 dB SNR. The ML algorithm misclassified 37 of the 50 distributed scattering centers at 10 dB and 2 of the 50 scattering centers at 20 dB. The fast variation misclassified 38 of the 50 distributed scattering centers at 10 dB and correctly classified all the distributed scattering centers at every other resolution. Only trials that correctly classified the scattering center were used to compute the variances of the parameter estimates. Improved region classification at low SNR could be realized by using a more statistically-based classifier, such as an MDL-based technique.

Figure 4 shows results in which we fixed the SNR at of 30 dB and evaluated algorithm performance at 3 in, 6 in, and 12 in resolutions. The estimates of the parameters of the localized scattering mechanisms and the x parameter of the distributed mechanism obtained with the ML algorithm are near the bound at 3 in, 6 in, and 12 in resolution. The y and L parameters of the distributed scattering mechanism are also near the bound for 6 in and 12 in resolution, but significantly above the bound for 3 in resolution. We attribute this to mismatch between the parametric model and measured data at this resolution. The estimates obtained from the fast variation of the algorithm are generally higher than the bound, but accurately describe the scattering centers. For example, the standard deviation of the estimate of the down range position of a localized scattering center at 12 in resolution and 30 dB SNR is less than 2 cm.

5.3. MSTAR Target Results

We present initial parameter estimation results on a measured spotlight mode SAR image of a T-72 tank at 15° depression, distributed by the MSTAR program[5] (chip number "HB05649.016"). The data was collected such that the barrel of the tank was broadside to the radar. This corresponds to an azimuth of 80.77°, where 0° is taken to be the front of the tank. This image is shown in Figure 5.

Figure 6 shows the results of applying both the ML and the fast algorithm to the tank image. Although quantitative analysis of feature accuracy is not possible, qualitative performance can be assessed from the reconstruction and fit error images. For the ML algorithm, 71% of the energy in the original image is accounted for by the simulated scattering centers. If we consider only the rectangular region at the center of the image that contains the tank, we find that the simulated scattering centers account for 85% of the energy of the target. For the fast algorithm, 61% of the energy in the full image and 69% of the energy in the smaller region occupied by the tank.

6. CONCLUSIONS

We have developed algorithms for automatic extraction of attributed scattering parameters from measured SAR imagery. Both an approximate ML and a computationally fast algorithm are presented. The algorithms include segmentation to isolate high-energy regions in SAR images that correspond to the scattering centers of target objects. We process the data in these regions and generate initial parameter estimates; we then optionally apply nonlinear minimization techniques to refine the estimates. These algorithms are completely automated and require no user intervention decompose a SAR image into a collection of physically descriptive parameters.

We have demonstrated the effectiveness of our algorithms on both simulated and measured SAR images. We used data generated directly from our parametric model and data generated using the Xpatch simulation system to demonstrate the ability of our algorithms to accurately estimate the parameters of scattering centers. We also used these data sets to demonstrate that the maximum likelihood algorithm achieves the Cramér-Rao lower bound on estimator variance in most cases. We used measured images of vehicles to demonstrate the ability of our algorithms to determine physical parameters that accurately describe the physical characteristics of those targets.

Current research is focused on reducing computation time and refining the order and structure selection components of the algorithm. Computation time is being reduced by refining initial estimates and normalizing the

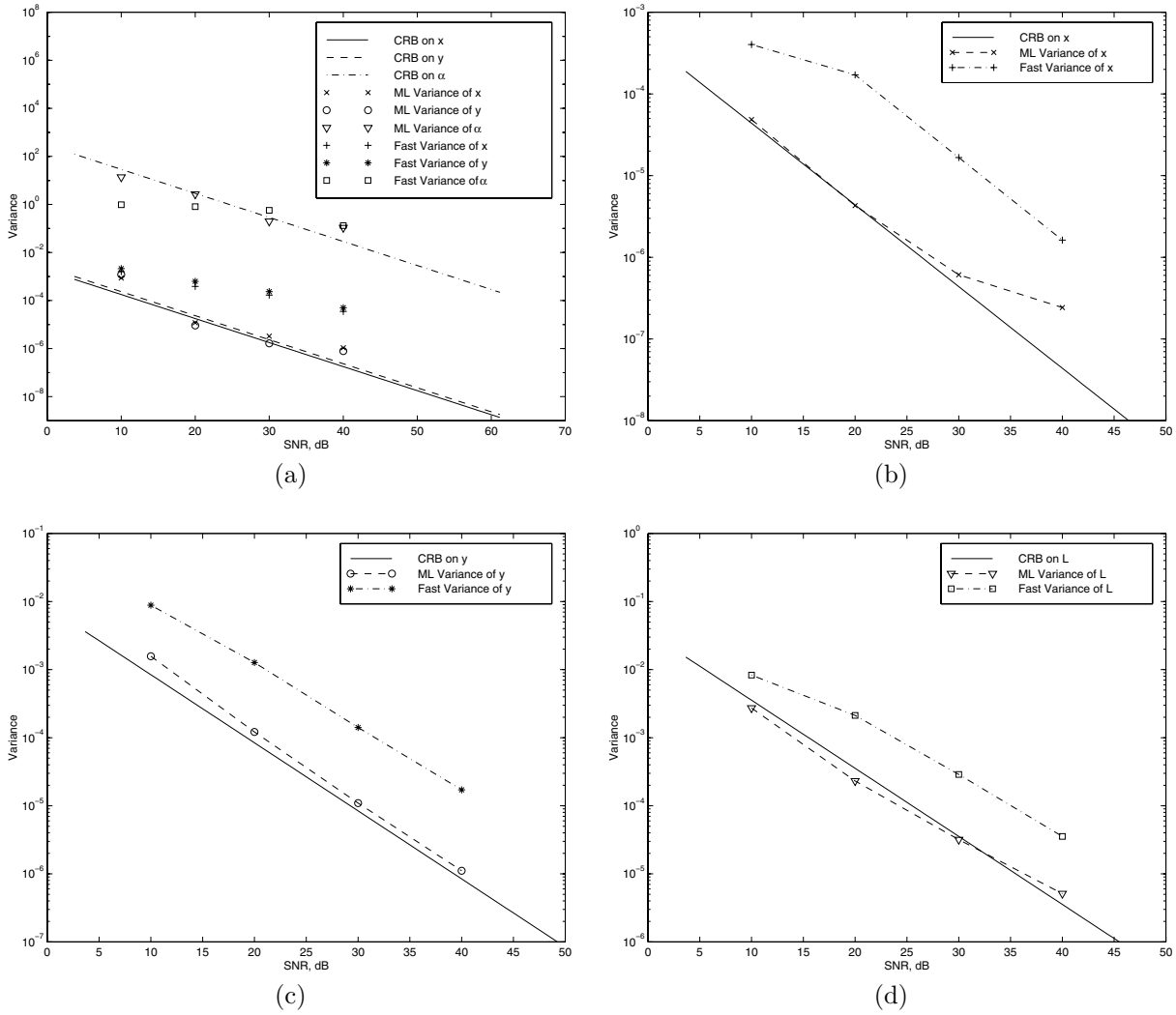

Figure 3. Observed Variances of ML and Fast Variations of the parameter estimation algorithm, for SLICY trihedral at 6" resolution. Variances of x and y are in in^2.

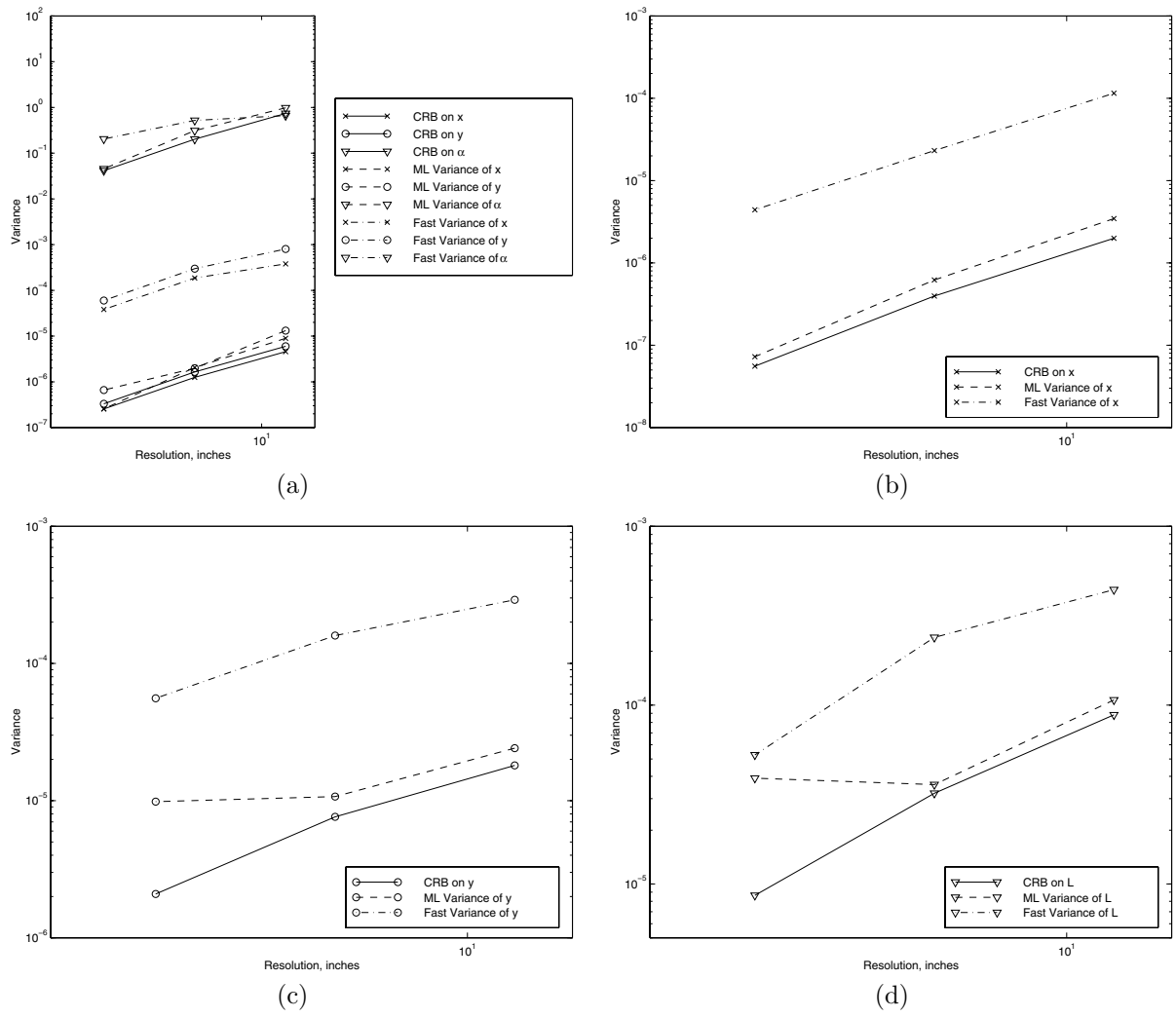

Figure 4. Observed Variances of ML and Fast Variations of the parameter estimation algorithm, for SLICY trihedral at 30 dB SNR and 3 in, 6 in, and 12 in resolutions. Variances of x and y are in in^2.

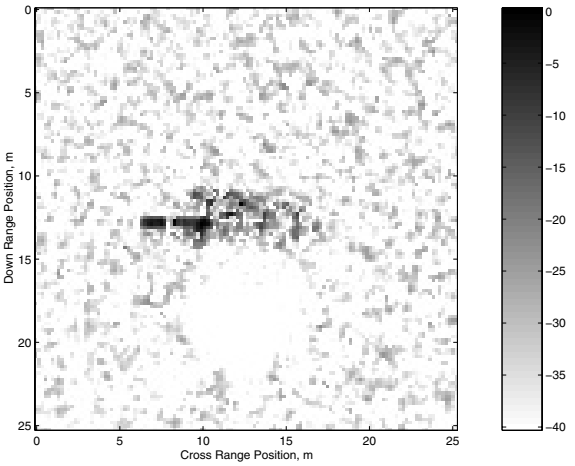

Figure 5. Measured SAR Image of T-72 Tank, in dB below the peak value

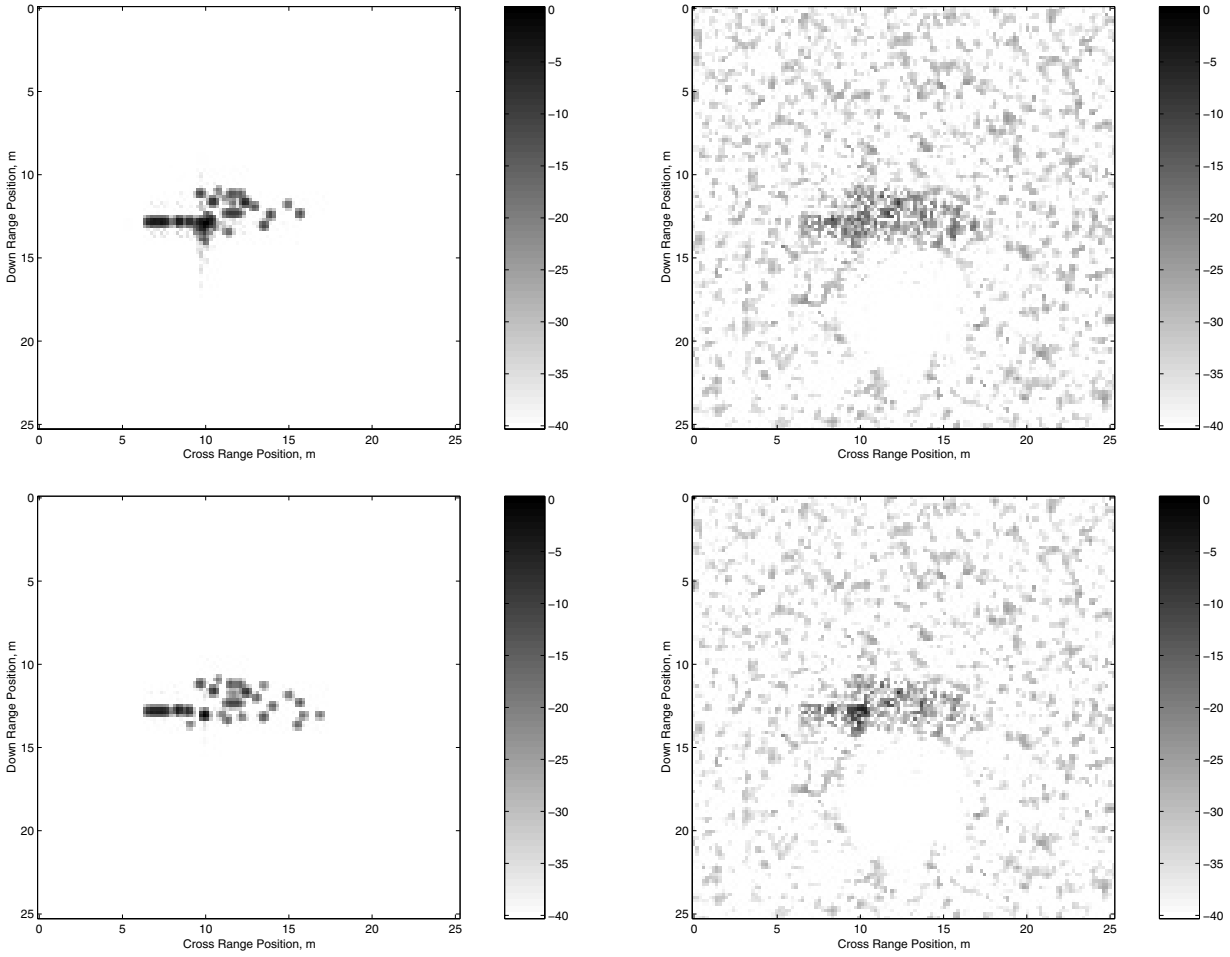

Figure 6. Reconstruction (left) and residual energy (right) of T-72 Tank. Top row: ML algorithm; bottom row: fast algorithm. Scale: magnitude in dB below the peak of the original tank image.

parameters before iterative refinement. We are also developing techniques to improve the probability of correct classification of a region as a distributed scattering center or as a single or multiple localized scattering centers. Also, larger-scale testing on SLICY and measured SAR data is underway.

REFERENCES

1. L. C. Potter and R. L. Moses, "Attributed scattering centers for SAR ATR," *IEEE Transactions on Image Processing* **6**, pp. 79–91, January 1997.
2. M. Gerry, *Two-dimensional inverse scattering based on the GTD model*. PhD thesis, The Ohio State University, Columbus, OH, 1997.
3. M. J. Gerry, L. C. Potter, I. J. Gupta, and A. van der Merwe, "A parametric model for synthetic aperture radar measurements," to appear in *IEEE Transactions on Antennas and Propagation*, 1999.
4. M.-W. Tu, I. Gupta, and E. Walton, "Application of maximum likelihood estimation to radar imaging," *IEEE Transactions on Antennas and Propagation* **45**(1), pp. 20–27, 1997.
5. "MSTAR (Public) Targets: T-72, BMP-2, BTR-70, SLICY," see http://www.mbvlab.wpafb.af.mil/public/MBVDATA.
6. J. J. Sacchini, W. M. Steedly, and R. L. Moses, "Two-dimensional Prony modeling and parameter estimation," *IEEE Transactions on Signal Processing* **41**, pp. 3127–3137, November 1993.
7. J. Stach and E. LeBaron, "Enhanced image editing by peak region segmentation," in *Proceedings of the 1996 AMTA Symposium*, October 1996.
8. J. Tsao and B. D. Steinberg, "Reduction of sidelobe and speckle artifacts in microwave imaging: The CLEAN technique," *IEEE Trans. Ant. Prop.* **36**, pp. 543–556, April 1988.
9. M. Koets, "Automated algorithms for extraction of physically relevant features from synthetic aperture radar imagery," Master's thesis, The Ohio State University, Columbus, OH, 1998.